IEEE Access
Multidisciplinary ⋮ Rapid Review ⋮ Open Access Journal

Received 20 February 2023, accepted 2 March 2023, date of publication 17 March 2023, date of current version 17 May 2023.

Digital Object Identifier 10.1109/ACCESS.2023.3258925

RESEARCH ARTICLE

Mode Switching Based Parameter Identification for 2TX-1RX Wireless Power Transfer Systems

KANG YUE[1,2,3,4], (Student Member, IEEE), YU LIU[1,5], (Senior Member, IEEE), MINFAN FU[1], (Senior Member, IEEE), JUNRUI LIANG[1], (Senior Member, IEEE), AND HAOYU WANG[1], (Senior Member, IEEE)

[1]School of Information Science and Technology, ShanghaiTech University, Shanghai 201210, China
[2]Shanghai Advanced Research Institute, Chinese Academy of Sciences, Shanghai 201210, China
[3]Shanghai Institute of Microsystem and Information Technology, Chinese Academy of Sciences, Shanghai 200050, China
[4]Shanghai Advanced Research Institute and Shanghai Institute of Microsystem and Information Technology, University of Chinese Academy of Sciences, Beijing 100049, China
[5]Key Laboratory of Control of Power Transmission and Conversion (SJTU), Ministry of Education, Shanghai 200240, China

Corresponding author: Yu Liu (liuyu@shanghaitech.edu.cn)

This work was supported in part by the National Natural Science Foundation of China under Grant 51807119; and in part by the Key Laboratory of Control of Power Transmission and Conversion (SJTU), Ministry of Education, under Grant 2022AB01.

ABSTRACT Parameters within wireless power transfer (WPT) systems could vary for different reasons. On one hand, mutual inductances and load conditions could vary due to different operating points of the WPT system. On the other hand, the values of capacitors within the WPT system could also vary due to aging issues. Identifying those parameters is of great importance to ensure highly efficient, controllable, and reliable operation for WPT systems. However, those parameters are strongly coupled within the system and are quite challenging to be estimated at the same time. This paper proposes a model based method to estimate all the parameters of interest, including mutual inductances, load condition, and all the capacitances, for multi-coil WPT systems with 2 transmitting coils (2TX) and 1 receiving coil (1RX). Specifically, to overcome the challenge of estimating many parameters at the same time, the idea of ''mode switching'' is applied to greatly improve the redundancy of the parameter identification problem. Auxiliary standard capacitors are introduced into the system to enable the switching of different operating modes. Afterward, a mathematical model is established to describe the physical laws among all the interested parameters in each mode, including the fundamental frequency and harmonic components. Finally, a standard solve procedure is introduced to solve the nonlinear model and calculate the parameters. The method only requires transmitter side measurements, without any information from the receiver side. Experiments conducted on a prototype of a 2TX-1RX LCC-S WPT system verified the effectiveness of the proposed parameter identification method.

INDEX TERMS Wireless power transfer (WPT), parameter identification, mutual inductances and load tracking, capacitor monitoring.

I. INTRODUCTION

Wireless power transfer (WPT) is widely used in electric vehicles, portable devices, implantable medical equipments, and underwater robots because of its safety and convenience [1], [2], [3], [4], [5]. Inductive WPT systems deliver energy from transmitters to receivers via the magnetic field. To track maximum energy transfer efficiency and realize constant current/voltage controls of WPT systems, knowledge of parameters including mutual inductances, loads, and other system parameters is crucial [6], [7], [8], [9], [10]. The mutual inductance between transmitting coil and receiving coil is subjected to the distance and orientation between coils. The load condition can also change with different electrical equipment. Also, during the operation of WPT systems, other circuit parameters such as the capacitances could vary due to aging issues, which will affect not only control objectives but also the reliable operation of the system [11], [12], [13]. As a result, monitoring the parameters is essential for WPT systems.

The associate editor coordinating the review of this manuscript and approving it for publication was Mauro Gaggero.

A. ESTIMATION OF MUTUAL INDUCTANCES AND LOADS

Wireless communication transmitting information (output voltage, current, load, duty cycle) between the transmitter and receiver is traditionally applied to monitor the mutual inductance and realize the output/efficiency control [10]. It requires receiver information with sensors embedded in the receiver side, which increases system complexity and cost, and causes time delay. To avoid communication with the receiver, researchers proposed estimation methods only with transmitter side information. Energy injection methods contain the energy injection phase and dissipation phase, and detect load information by analyzing the amplitude decay rate of the inductor current during the energy dissipation transient process [14], [15]. They require the inductance, resistance, and current signal. Impedance model based parameter identification methods are widely applied for WPT [16], [17], [18]. Model based methods make full use of the system topology and build the model containing state equations or KCL/KVL equations to analyze the relationship among the equivalent impedance, parameters of interest and system measurements. Study [16] obtains the mutual inductance by analyzing the relationship between the transfer function and the parameters with only transmitter side information for SS (series compensation for transmitter and receiver) WPT system. Studies [17], [18] obtain the mutual inductance with a differential equation model in time domain. To identify the mutual inductance and load simultaneously, references [19], [20] attached additional inverters/capacitors to the SS system to provide more information related to parameters by switching auxiliary components. Various references also make full use of frequency information. In [21] and [22], the frequency sweep method is applied to provide more information for equivalent impedances, mutual inductances, and loads in SS systems. Study [23] simplifies the system with high order harmonic (5^{th}) and calculates the mutual inductance accurately only with transmitter current. In [24] and [25], harmonics information including inter-harmonics and high-order harmonics is applied to identify the mutual inductance and load by generating sets of equations related to impedances and parameters.

Compared to WPT systems containing one transmitting coil and one receiving coil, multi-coil WPT systems are proposed for larger charging areas and higher power applications. For multi-coil systems, the mutual couplings among coils are more complex, resulting in more parameters to be identified, such as multiple mutual inductances between each transmitter and receiver, and cross coupling between two transmitters or between two receivers. A very limited number of studies explore the estimation method for multi-coil systems. In [26], the frequency sweep method and adaptive algorithm are applied to monitor mutual inductances and loads. In [27], [28], and [29], the mutual inductance ratio is calculated with the reflected resistance and coil current. With receiver side output, the mutual inductances can be calculated and the maximum efficiency can be achieved for multi-transmitter systems. Study [30] also utilizes the load information and currents through coils to calculate the mutual inductances and realize maximum efficiency control for the multi-transmitter system. From the above literature, the challenge for the estimation method is to estimate more parameters accurately, with no feedback signal from the receiver, and minimize the use of sensors and additional components as possible. The key point is to improve information redundancy and generate more sets of equations related to parameters.

B. ESTIMATION OF CAPACITANCES

Device aging and degradation usually occur in power electronic systems during long-time operation, affecting system operational reliability and performance (output, efficiency, and devices stress) [11], [12], [13]. What's more, parameter deviation could potentially cause large estimation errors for the model based estimation method [25]. Among various components of power electronic systems, the capacitor is one of the most vulnerable devices [31]. As a result, monitoring the values of capacitors is also crucial for WPT systems. Capacitor monitoring methods can be mainly classified into observer-based methods and parameter identification based methods. Studies [32], [33] monitor the whole system's healthy condition including variations of inductances and capacitances by checking the consistency between the model and measurements. In [34], [35], and [36], the capacitor value is calculated and the fault is detected by comparing the calculated value and the normal value. For WPT systems, parameter identification based methods could be adopted. The idea is to add the capacitances as additional states to be identified and calculate the states including mutual inductances, loads, and capacitances simultaneously. If the capacitances have not been modeled, the variations of the capacitance will not be considered in the model, and inaccuracies of capacitances will propagate to the values of other parameters. Frequency sweep based method could be used to generate more equations about states during different frequencies [26], [37]. However, it needs to sweep the operating frequency in a reasonable range.

To sum up, to ensure highly efficient, controllable and reliable operation of WPT systems, estimation of mutual inductances, load and capacitances at the same time is challenging. Other parameters of the system such as the self-inductances are assumed to be known constants since they typically do not suffer from aging issues as capacitors. The number of unknown parameters could even increase for multi-coil WPT systems. This paper takes a two-transmitter-one-receiver (2TX-1RX) LCC-S compensated system as an example, which has 2 mutual inductances between TX and RX, a load condition, and 5 unknown capacitances to be estimated. To improve the redundancy of the parameter identification problem, auxiliary standard capacitors with known values of capacitances are added to the resonant tank, to formulate various operational modes. What's more, in each mode, the physical laws at the fundamental frequency and high-order

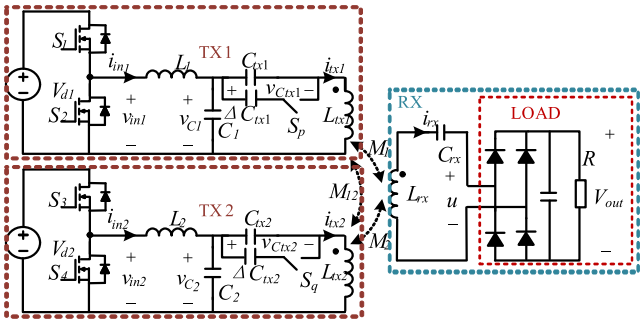

FIGURE 1. Equivalent circuit of 2TX-1RX LCC-S WPT system.

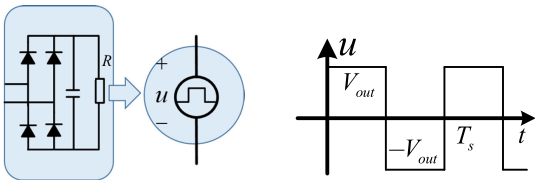

(a) Rectifier and load (b) Waveforms of u

FIGURE 2. Square wave equivalence of the rectifier and load.

harmonics are considered to further improve redundancy. With the overall model of the system with interested parameters as unknowns, a nonlinear state estimator is applied to solve the parameters. The primary contributions of the paper are summarized below,

1) It only requires voltage measurements at the transmitter side, without the requirement of any current sensors or receiver side information to minimize system complexity;
2) Only two auxiliary capacitors are required to generate various operational modes; it does not require additional hardware or frequency sweeping of the system;
3) Extensive experimental results prove that the proposed method can accurately estimate the full package of parameters of interest, including mutual inductances, load condition, and 5 unknown capacitances at the same time, with various operating conditions of the system.

The rest of the paper is arranged as follows. Section II derives the model of the 2TX-1RX LCC-S WPT system with all unknown parameters as states of the system. Section III adopts a nonlinear state estimator to obtain unknown parameters. Section IV presents hardware experiments to validate the proposed method under various scenarios. Section V adds a discussion. Section VI draws a conclusion.

II. MODEL DERIVATION FOR PARAMETER IDENTIFICATION

A. CHARACTERISTICS OF 2TX-1RX LCC-S WPT SYSTEM

Fig.1 shows the topology of a 2TX-1RX LCC-S WPT system, containing two transmitting coils and one receiving coil. The system contains inverter circuits converting dc to ac, transmitting/receiving coils and compensated capacitors delivering power, and rectifier circuit converting ac to dc.

TABLE 1. Mode generation with auxiliary capacitors.

Index	Status of switches	Values of two capacitors
Mode 1	S_p off, S_q off	C_{tx1}, C_{tx2}
Mode 2	S_p on, S_q off	$(C_{tx1}+\Delta C_{tx1}), C_{tx2}$
Mode 3	S_p off, S_q on	$C_{tx1}, (C_{tx2}+\Delta C_{tx2})$

V_{d1} and V_{d2} are the dc power supplies. S_1, S_2, S_3, and S_4 are MOSFET switches for the two half-bridge inverters. L_{tx1}, L_{tx2}, and L_{rx} are self-inductances of coils. L_1 and L_2 are compensation inductors. C_1, C_2 and C_{tx1}, C_{tx2}, C_{rx} are compensation capacitors. M_1 and M_2 are mutual inductances between each transmitting coil and receiving coil. M_{12} is the cross coupling between transmitting coils. R is the load. v_{in1}, v_{in2} and i_{in1}, i_{in2} are input voltages and currents of two transmitters, respectively. v_{C_1} and v_{C_2} are voltages across capacitors C_1 and C_2, respectively. $v_{C_{tx1}}$ and $v_{C_{tx2}}$ are voltages across the capacitors C_{tx1} and C_{tx2}, respectively. $v_{L_{tx1}}$, $v_{L_{tx2}}$ and i_{tx1}, i_{tx2} are voltages across and currents flowing through the transmitting coils, respectively. u and i_{rx} are the input voltage and current of the rectifier, respectively. Fig.2 shows the equivalent circuit of rectifier and the load. It is simplified as a pure square wave voltage source with an amplitude equals to the DC output voltage V_{out}.

For the design of the ideal parameters of the WPT system, the transmitters and receiver are both fully resonant at ω_0,

$$\begin{aligned} &\omega_0 L_1 = 1/(\omega_0 C_1), \quad \omega_0 L_2 = 1/(\omega_0 C_2), \\ &\omega_0 L_{rx} = 1/(\omega_0 C_{rx}) \\ &\omega_0 L_{tx1} = \frac{1}{\omega_0 C_{tx1}} + \frac{1}{\omega_0 C_1}, \quad \omega_0 L_{tx2} = \frac{1}{\omega_0 C_{tx2}} + \frac{1}{\omega_0 C_2} \end{aligned} \tag{1}$$

where $\omega_0 = 2\pi f_0$, and f_0 is the resonant frequency. Note that (1) describes the relationship among ideal parameters of the system. During the operation of the system, due to the aging of capacitors, the true values of C_1, C_2, C_{tx1}, C_{tx2}, and C_{rx} of the system could deviate from the ideal values. Also, unlike the capacitors within the system, since the inductors do not quite suffer from aging, the values of self-inductances within the system are typically assumed to be known constants.

To generate different operating modes of the WPT system, here two auxiliary capacitors ΔC_{tx1} and ΔC_{tx2} are added to the system as standard components, as shown in Fig. 1. ΔC_{tx1} and ΔC_{tx2} are connected in parallel with two compensation capacitors C_{tx1} and C_{tx2}, respectively. Switches S_p and S_q are connected to capacitors ΔC_{tx1} and ΔC_{tx2} to provide more operating modes by switching on/off. With the two auxiliary capacitors, here three example operating modes are generated in Table 1. Note that the 4th operating mode with both switches on is not adopted in the paper since the redundancy is sufficient to estimate all the interested parameters.

In mode 1, switches S_p and S_q are off. The system works in normal conditions. In mode 2, the switch S_p is on and S_q is off; the parameter C_{tx1} will change from C_{tx1} to $C_{tx1}+\Delta C_{tx1}$.

In mode 3, the switch S_q is on and S_p is off; the parameter C_{tx2} will change from C_{tx2} to $C_{tx2} + \Delta C_{tx2}$.

B. SYSTEM MODEL FOR EACH OPERATING MODE

The mathematical model for each operating mode is derived as follows.

1) MODE 1

In this mode, the system operates in normal condition. The modeling procedure is to describe the physical laws (including KCL, KVL, and characteristics of each component) that the system should obey. Since the output of the inverter v_{in1}, v_{in2}, and the input of the rectifier u are regulated as nearly square wave signals, there exists some high-order harmonics in the circuit even after resonant filtering. The equation set (2) shows the KCL and KVL laws of the coils for the n^{th} harmonic in the frequency domain, where $n \geq 1$ is an integer.

$$\begin{aligned}
&\tilde{V}_{in1}^{n^{th}} = jn\omega L_1 \tilde{I}_{in1}^{n^{th}} + \tilde{V}_{C_1}^{n^{th}}, \quad \tilde{V}_{in2}^{n^{th}} = jn\omega L_2 \tilde{I}_{in2}^{n^{th}} + \tilde{V}_{C_2}^{n^{th}} \\
&\tilde{I}_{in1}^{n^{th}} = \tilde{I}_{tx1}^{n^{th}} \\
&\qquad + jn\omega C_1 \tilde{V}_{C_1}^{n^{th}}, \quad \tilde{I}_{in2}^{n^{th}} = \tilde{I}_{tx2}^{n^{th}} + jn\omega C_2 \tilde{V}_{C_2}^{n^{th}} \\
&\tilde{V}_{C_1}^{n^{th}} = (1/(jn\omega C_{tx1}) + jn\omega L_{tx1} + r_{tx1})\tilde{I}_{tx1}^{n^{th}} - jn\omega M_1 \tilde{I}_{rx}^{n^{th}} \\
&\qquad + jn\omega M_{12} \tilde{I}_{tx2}^{n^{th}} \\
&\tilde{V}_{C_2}^{n^{th}} = (1/(jn\omega C_{tx2}) + jn\omega L_{tx2} + r_{tx2})\tilde{I}_{tx2}^{n^{th}} - jn\omega M_2 \tilde{I}_{rx}^{n^{th}} \\
&\qquad + jn\omega M_{12} \tilde{I}_{tx1}^{n^{th}} \\
&\tilde{U}^{n^{th}} = jn\omega M_1 \tilde{I}_{tx1}^{n^{th}} + jn\omega M_2 \tilde{I}_{tx2}^{n^{th}} \\
&\qquad - \tilde{I}_{rx}^{n^{th}} (jn\omega L_{rx} - j/(n\omega C_{rx}) + r_{rx})
\end{aligned} \tag{2}$$

In (2), the symbol $(\tilde{\bullet})^{n^{th}}$ means the n^{th} harmonic component of the variable $(\bullet)$ in complex form. ω is the actual operating angular frequency of the system, which could be different from the resonant frequency. r_{tx1}, r_{tx2} and r_{rx} are the equivalent series resistances of TX1, TX2 and RX coils, respectively. The main purpose of modeling is to find the relationship among the available measurements and the parameters of interest (including unknown internal states, mutual inductances, load, and capacitances). Here, set v_{in1}, v_{in2} and v_{C_1}, v_{C_2} as measurements of the system. With those measurements, the currents through the inductors i_{in1}, i_{in2} can be calculated directly from the physical laws of the inductors L_1 and L_2. For the phasor domain expression of the n^{th} harmonic component, the way of calculating $\tilde{I}_{in1}^{n^{th}}$ and $\tilde{I}_{in2}^{n^{th}}$ using measurements $\tilde{V}_{in1}^{n^{th}}$, $\tilde{V}_{in2}^{n^{th}}$, $\tilde{V}_{C_1}^{n^{th}}$ and $\tilde{V}_{C_2}^{n^{th}}$ is shown in the first row of (2). Through this procedure, the system only needs voltage sensors and avoids the complexity of using current sensors. The currents $\tilde{I}_{tx1}^{n^{th}}$ and $\tilde{I}_{tx2}^{n^{th}}$ through transmitting coils can be calculated as,

$$\tilde{I}_{tx1}^{n^{th}} = jn\omega C_{tx1} \tilde{V}_{C_{tx1}}^{n^{th}}, \quad \tilde{I}_{tx2}^{n^{th}} = jn\omega C_{tx2} \tilde{V}_{C_{tx2}}^{n^{th}} \tag{3}$$

Substitute (3) into (2), and the capacitances C_{tx1} and C_{tx2} in the denominator can be removed. Additional states $\tilde{V}_{C_{tx1}}^{n^{th}}$ and $\tilde{V}_{C_{tx2}}^{n^{th}}$ are introduced and states $\tilde{I}_{tx1}^{n^{th}}$ and $\tilde{I}_{tx2}^{n^{th}}$ are eliminated. Finally, there are 5 complex equations at each order harmonics for modeling.

Next, additional modeling for the pure square wave power supply $\tilde{U}^{n^{th}}$ of load part is introduced. The periodic function $u(t)$ in Fig. 2 (b) can be expressed in Fourier series form as follows, composed of multiple harmonics,

$$u(t) = \sum_{n=1,3,5,\ldots} \left[\frac{4V_{out}}{n\pi} \sin(n\omega t + \theta_n) \right] \tag{4}$$

where the fundamental frequency and n^{th} harmonic components of $u(t)$ are defined as $u_1(t) = \frac{4V_{out}}{\pi} \sin(\omega t + \theta_1)$ and $u_n(t) = \frac{4V_{out}}{n\pi} \sin(n(\omega t + \frac{\theta_n}{n}))$. The phasor relationship between the fundamental frequency and n^{th} harmonic component of $u(t)$ is shown in (5),

$$\begin{aligned}
U_1 &= nU_n \\
\theta_1 &= \theta_n / n
\end{aligned} \tag{5}$$

where $U_1 = 4V_{out}/\pi$ and $U_n = 4V_{out}/n/\pi$ are magnitudes of fundamental and n^{th} harmonic components of $u(t)$. θ_1 and θ_n are the initial phase angles of $u_1(t)$ and $u_n(t)$, respectively.

As a result, for each mode, the model contains the physical law in (2) with the fundamental frequency component and harmonic components, and the relationship between the fundamental frequency and harmonic components of square wave $u(t)$ in (5). The complex equation in (2) can be separated into real and imaginary parts. Since the magnitude of higher order components is rather small, here only the fundamental frequency and 3$^{\text{rd}}$ harmonic components are taken into consideration for modeling. In (2) and (5), the variable n will be set as 1 and 3. Considering (2), (3) and (5), the model for mode 1 is shown in (6),

$$\begin{aligned}
I_{in1,r}^1 &= -\omega(C_{tx1} V_{C_{tx1},i}^1 + C_1 V_{C_1,i}^1), \\
I_{in1,i}^1 &= \omega(C_{tx1} V_{C_{tx1},r}^1 + C_1 V_{C_1,r}^1) \\
I_{in2,r}^1 &= -\omega(C_{tx2} V_{C_{tx2},i}^1 + C_2 V_{C_2,i}^1), \\
I_{in2,i}^1 &= \omega(C_{tx2} V_{C_{tx2},r}^1 + C_2 V_{C_2,r}^1) \\
0 &= -\omega^2 L_{tx1} C_{tx1} V_{C_{tx1},r}^1 + \omega M_1 I_{rx,i}^1 - r_{tx1}\omega C_{tx1} V_{C_{tx1},i}^1 \\
&\quad - V_{L_{tx1},r}^1 \\
0 &= -\omega^2 L_{tx1} C_{tx1} V_{C_{tx1},i}^1 - \omega M_1 I_{rx,r}^1 + r_{tx1}\omega C_{tx1} V_{C_{tx1},r}^1 \\
&\quad - V_{L_{tx1},i}^1 \\
0 &= -\omega^2 L_{tx2} C_{tx2} V_{C_{tx2},r}^1 + \omega_s M_2 I_{rx,i}^1 - r_{tx2}\omega C_{tx2} V_{C_{tx2},i}^1 \\
&\quad - V_{L_{tx2},r}^1 \\
0 &= -\omega^2 L_{tx2} C_{tx2} V_{C_{tx2},i}^1 - \omega M_2 I_{rx,r}^1 + r_{tx2}\omega C_{tx2} V_{C_{tx2},r}^1 \\
&\quad - V_{L_{tx2},i}^1 \\
0 &= \omega^2 M_1 C_{tx1} V_{C_{tx1},r}^1 + I_{rx,r}^1 r_{rx} + \omega^2 M_2 C_{tx2} V_{C_{tx2},r}^1 \\
&\quad - I_{rx,i}^1 Z_{r1} + U_1 \cos\theta_1 \\
0 &= \omega^2 M_1 C_{tx1} V_{C_{tx1},i}^1 + I_{rx,i}^1 r_{rx} + \omega^2 M_2 C_{tx2} V_{C_{tx2},i}^1 \\
&\quad + I_{rx,r}^1 Z_{r1} + U_1 \sin\theta_1
\end{aligned}$$

$$
\begin{aligned}
I_{in1,r}^{3^{rd}} &= -3\omega(C_{tx1}V_{C_{tx1},i}^{3^{rd}} + C_1V_{C_1,i}^{3^{rd}}),\\
I_{in1,i}^{3^{rd}} &= 3\omega(C_{tx1}V_{C_{tx1},r}^{3^{rd}} + C_1V_{C_1,r}^{3^{rd}})\\
I_{in2,r}^{3^{rd}} &= -3\omega(C_{tx2}V_{C_{tx2},i}^{3^{rd}} + C_2V_{C_2,i}^{3^{rd}}),\\
I_{in2,i}^{3^{rd}} &= 3\omega(C_{tx2}V_{C_{tx2},r}^{3^{rd}} + C_2V_{C_2,r}^{3^{rd}})\\
0 &= -3^2\omega^2L_{tx1}C_{tx1}V_{C_{tx1},r}^{3^{rd}} + 3\omega M_1I_{rx,i}^{3^{rd}}\\
&\quad - 3\omega r_{tx1}C_{tx1}V_{C_{tx1},i}^{3^{rd}} - V_{L_{tx1},r}^{3^{rd}}\\
0 &= -3^2\omega^2L_{tx1}C_{tx1}V_{C_{tx1},i}^{n^{3rd}} - 3\omega M_1I_{rx,r}^{3^{rd}}\\
&\quad + 3\omega r_{tx1}C_{tx1}V_{C_{tx1},r}^{3^{rd}} - V_{L_{tx1},i}^{3^{rd}}\\
0 &= -3^2\omega^2L_{tx2}C_{tx2}V_{C_{tx2},r}^{3^{rd}} + 3\omega_sM_2I_{rx,i}^{3^{rd}}\\
&\quad - 3\omega r_{tx2}C_{tx2}V_{C_{tx2},i}^{3^{rd}} - V_{L_{tx2},r}^{3^{rd}}\\
0 &= -3^2\omega^2L_{tx2}C_{tx2}V_{C_{tx2},i}^{3^{rd}} - 3\omega M_2I_{rx,r}^{3^{rd}}\\
&\quad + 3\omega r_{tx2}C_{tx2}V_{C_{tx2},r}^{3^{rd}} - V_{L_{tx2},i}^{3^{rd}}\\
0 &= 3^2\omega^2(M_1C_{tx1}V_{C_{tx1},r}^{3^{rd}} + M_2C_{tx2}V_{C_{tx2},r}^{3^{rd}}) + I_{rx,r}^{n^{th}}r_{rx}\\
&\quad - I_{rx,i}^{3^{rd}}Z_{r3} + U_3\cos\theta_3\\
0 &= 3^2\omega^2(M_1C_{tx1}V_{C_{tx1},i}^{3^{rd}} + M_2C_{tx2}V_{C_{tx2},i}^{3^{rd}}) + I_{rx,i}^{n^{th}}r_{rx}\\
&\quad + I_{rx,r}^{3^{rd}}Z_{r3} + U_3\sin\theta_3\\
0 &= U_1 - 3U_3, \quad 0 = 3\theta_1 - \theta_3
\end{aligned}
\tag{6}
$$

where $Z_{rn} = \left(n\omega L_{rx} - 1/(n\omega C_{rx})\right)$, $V_{L_{tx1}}^{n^{th}} = V_{C_1}^{n^{th}} - V_{C_{tx1}}^{n^{th}}$, $V_{L_{tx2}}^{n^{th}} = V_{C_2}^{n^{th}} - V_{C_{tx2}}^{n^{th}}$, $U_r^{n^{th}} = U_n\cos\theta_n$, $U_i^{n^{th}} = U_n\sin\theta_n$ and $n = 1$ and 3. U_n and θ_n are the magnitude and initial phase angle of $\tilde{U}^{n^{th}}$, respectively. Symbols $(\bullet)_r^{n^{th}}$ and $(\bullet)_i^{n^{th}}$ represent the real and imaginary parts of the variable $(\tilde{\bullet})^{n^{th}}$, respectively. In model (6), the cross coupling M_{12} is eliminated since the cross coupling M_{12} can usually be set as 0 with reasonable coil arrangement in practice or can be measured offline as a known parameter [38].

To sum up, for model (6), the values of $\tilde{V}_{in1}^{n^{th}}$, $\tilde{V}_{in2}^{n^{th}}$, $\tilde{V}_{C_1}^{n^{th}}$ and $\tilde{V}_{C_2}^{n^{th}}$ are measured, while the values of $\tilde{I}_{in1}^{n^{th}}$ and $\tilde{I}_{in2}^{n^{th}}$ are calculated via the first row of (2). The operating fundamental frequency ω and inductances (L_1, L_2, L_{tx1}, L_{tx2}, and L_{rx}) are known. In (6), there is a total of 22 real equations. The number of unknown states to be estimated is 23, including 7 parameters (M_1, M_2, C_1, C_2, C_{tx1}, C_{tx2}, C_{rx}) and 8 internal complex states (16 real states, including $V_{L_{tx1},r}^1$, $V_{L_{tx1},i}^1$, $V_{L_{tx2},r}^1$, $V_{L_{tx2},i}^1$, $I_{rx,r}^1$, $I_{rx,i}^1$, U_1, θ_1, $V_{L_{tx1},r}^{3^{rd}}$, $V_{L_{tx1},i}^{3^{rd}}$, $V_{L_{tx2},r}^{3^{rd}}$, $V_{L_{tx2},i}^{3^{rd}}$, $I_{rx,r}^{3^{rd}}$, $I_{rx,i}^{3^{rd}}$, U_3, and θ_3). Model (6) is a function including sets of equations related to the parameters to be identified. However, the 23 states cannot be solved because the number of states is larger than the number of equations with only mode 1. More modes to generate additional sets of equations are introduced as follows.

2) MODE 2

In mode 2, the switch S_p is on and S_q is off. The value of C_{tx1} is updated as $C_{tx1} + \Delta C_{tx1}$. The operating condition of the system will change, generating more information different from mode 1. The modeling procedure is similar to that in mode 1. First, similar to (2), demonstrate the KCL and KVL laws of the coils with the n^{th} harmonic component in the frequency domain as (7). Compared to (2) of mode 1, model (7) contains new items related to ΔC_{tx1}.

$$
\begin{aligned}
\tilde{I}_{in1}^{n^{th}} &= jn\omega_sC_{tx1}\tilde{V}_{C_{tx1}}^{n^{th}} + jn\omega C_1\tilde{V}_{C_1}^{n^{th}} + jn\omega_s\Delta C_{tx1}\tilde{V}_{C_{tx1}}^{n^{th}}\\
\tilde{I}_{in2}^{n^{th}} &= jn\omega_sC_{tx2}\tilde{V}_{C_{tx2}}^{n^{th}} + jn\omega_sC_2\tilde{V}_{C_2}^{n^{th}}\\
0 &= (jn\omega_sL_{tx1} + r_{tx1})jn\omega_sC_{tx1}\tilde{V}_{C_{tx1}}^{n^{th}} - jn\omega_sM_1\tilde{I}_{rx}^{n^{th}} - \tilde{V}_{L_{tx1}}^{n^{th}}\\
&\quad + (-n^2\omega_s^2L_{tx1} + jn\omega_sr_{tx1})\tilde{V}_{C_{tx1}}^{n^{th}}\Delta C_{tx1}\\
0 &= (jn\omega_sL_{tx2} + r_{tx2})jn\omega_sC_{tx2}\tilde{V}_{C_{tx2}}^{n^{th}} - jn\omega_sM_2\tilde{I}_{rx}^{n^{th}} - \tilde{V}_{L_{tx2}}^{n^{th}}\\
0 &= n^2\omega_s^2M_1C_{tx1}\tilde{V}_{C_{tx1}}^{n^{th}} + n^2\omega_s^2M_2C_{tx2}\tilde{V}_{C_{tx2}}^{n^{th}} + \tilde{U}^{n^{th}}\\
&\quad + \tilde{I}_{rx}^{n^{th}}(jn\omega_sL_{rx} - j/(n\omega_sC_{rx}) + r_{rx})\\
&\quad + n^2\omega_s^2M_1\Delta C_{tx1}\tilde{V}_{C_{tx1}}^{n^{th}}
\end{aligned}
\tag{7}
$$

The next step is to expand the complex equations of (7) into real and imaginary parts, and set n as 1 and 3. Similar to (6), considering the fundamental, 3rd harmonic information of physical laws, and the relation between fundamental and 3rd harmonic of $u(t)$, the model for mode 2 can be generated and is not shown here due to space limitations. In mode 2, similar to the analysis of mode 1, there are 22 equations and 23 states to be identified. M_1, M_2, C_1, C_2, C_{tx1}, C_{tx2}, and C_{rx} are 7 parameters, which are identical to that in mode 1. The internal complex states (16 real states, including $V_{L_{tx1},r}^1$, $V_{L_{tx1},i}^1$, $V_{L_{tx2},r}^1$, $V_{L_{tx2},i}^1$, $I_{rx,r}^1$, $I_{rx,i}^1$, U_1, θ_1, $V_{L_{tx1},r}^{3^{rd}}$, $V_{L_{tx1},i}^{3^{rd}}$, $V_{L_{tx2},r}^{3^{rd}}$, $V_{L_{tx2},i}^{3^{rd}}$, $I_{rx,r}^{3^{rd}}$, $I_{rx,i}^{3^{rd}}$, U_3, and θ_3) are new states different from those in mode 1 because the operating condition has changed.

3) MODE 3

In mode 3, the switch S_p is off and S_q is on. The value of C_{tx2} is updated as $C_{tx2} + \Delta C_{tx2}$. Similar to (2) and (7), the KCL and KVL laws of the coils with the n^{th} harmonic component for mode 3 are shown in (8), with a new item related to ΔC_{tx2}.

$$
\begin{aligned}
\tilde{I}_{in1}^{n^{th}} &= jn\omega_sC_{tx1}\tilde{V}_{C_{tx1}}^{n^{th}} + jn\omega C_1\tilde{V}_{C_1}^{n^{th}}\\
\tilde{I}_{in2}^{n^{th}} &= jn\omega_sC_{tx2}\tilde{V}_{C_{tx2}}^{n^{th}} + jn\omega_sC_2\tilde{V}_{C_2}^{n^{th}} + jn\omega_s\Delta C_{tx2}\tilde{V}_{C_{tx2}}^{n^{th}}\\
0 &= (jn\omega_sL_{tx1} + r_{tx1})jn\omega_sC_{tx1}\tilde{V}_{C_{tx1}}^{n^{th}} - jn\omega_sM_1\tilde{I}_{rx}^{n^{th}} - \tilde{V}_{L_{tx1}}^{n^{th}}\\
0 &= (jn\omega_sL_{tx2} + r_{tx2})jn\omega_sC_{tx2}\tilde{V}_{C_{tx2}}^{n^{th}} - jn\omega_sM_2\tilde{I}_{rx}^{n^{th}} - \tilde{V}_{L_{tx2}}^{n^{th}}\\
&\quad + (-n^2\omega_s^2L_{tx2} + jn\omega_sr_{tx2})\tilde{V}_{C_{tx2}}^{n^{th}}\Delta C_{tx2}\\
0 &= n^2\omega_s^2M_1C_{tx1}\tilde{V}_{C_{tx1}}^{n^{th}} + n^2\omega_s^2M_2C_{tx2}\tilde{V}_{C_{tx2}}^{n^{th}} + \tilde{U}^{n^{th}}\\
&\quad + \tilde{I}_{rx}^{n^{th}}(jn\omega_sL_{rx} - j/(n\omega_sC_{rx}) + r_{rx})\\
&\quad + n^2\omega_s^2M_2\Delta C_{tx2}\tilde{V}_{C_{tx2}}^{n^{th}}
\end{aligned}
\tag{8}
$$

Similar to mode 2, the model for mode 3 can be generated by expanding (8) into real and imaginary parts, setting $n = 1$, 3, and adding additional relation (5). The final form is similar to those in (6). Still, 22 equations and 23 states (including 7 parameters and 16 real states).

C. COMBINED MODEL FOR PARAMETER IDENTIFICATION

For each mode, the number of equations is 22, and the number of states to be estimated is 23. After combining the models of all three modes, the combined model is composed of 66 equations; the state vector contains the 7 parameters (M_1, M_2, C_1, C_2, C_{tx1}, C_{tx2}, and C_{rx}) and 48 (16*3) internal states of three modes ($V^1_{L_{tx1},r}$, $V^1_{L_{tx1},i}$, $V^1_{L_{tx2},r}$, $V^1_{L_{tx2},i}$, $I^1_{rx,r}$, $I^1_{rx,i}$, U_1, θ_1, $V^{3rd}_{L_{tx1},r}$, $V^{3rd}_{L_{tx1},i}$, $V^{3rd}_{L_{tx2},r}$, $V^{3rd}_{L_{tx2},i}$, $I^{3rd}_{rx,r}$, $I^{3rd}_{rx,i}$, U_3, and θ_3 of each mode), i.e., totally 55 states. The combined model for parameter identification is rewritten in the following standard format,

$$z = h(\boldsymbol{x}) \tag{9}$$

where $\boldsymbol{z} \in \boldsymbol{R}^{66\times 1}$ is the measurement vector, containing the fundamental and 3rd harmonic components of v_{in1}, v_{in2}, v_{C_1}, v_{C_2}, i_{in1} and i_{in2} in three operating modes, as well as zeros. $\boldsymbol{x} \in \boldsymbol{R}^{55\times 1}$ is the state vector.

III. NONLINEAR STATE ESTIMATOR FOR PARAMETERS

Next, the nonlinear overdetermined equations in (9) can be solved via a nonlinear state estimator. The parameter identification problem can be converted into an optimization problem with the idea of weighted least square,

$$\min_{\boldsymbol{x}} J = (\boldsymbol{h}(\boldsymbol{x}) - \boldsymbol{z})^{\mathrm{T}} \boldsymbol{W} (\boldsymbol{h}(\boldsymbol{x}) - \boldsymbol{z}) \tag{10}$$

The optimization problem is to find an optimal solution $\hat{\boldsymbol{x}}$, which minimizes the weighted sum of squares of residuals. The solution $\hat{\boldsymbol{x}}$ should obey $\partial J/\partial \boldsymbol{x} = 0$, a set of nonlinear equations. The Newton-Raphson method is an effective way to solve nonlinear algebraic equations and can be applied to solve the problem [39], [40]. The best-estimated state vector $\hat{\boldsymbol{x}}$ can be obtained with the iteration in (11) until convergence,

$$\boldsymbol{x}^{\nu+1} = \boldsymbol{x}^{\nu} - (\boldsymbol{H}^T \boldsymbol{W} \boldsymbol{H})^{-1} \boldsymbol{H}^T \boldsymbol{W} (h(\boldsymbol{x}^{\nu}) - \boldsymbol{z}) \tag{11}$$

where $\boldsymbol{H} = \partial \boldsymbol{h} / \partial \boldsymbol{x}\big|_{\boldsymbol{x}=\boldsymbol{x}^{\nu}}$ is the Jacobian matrix evaluated at $\boldsymbol{x} = \boldsymbol{x}^{\nu}$. $\boldsymbol{W}$ is the weight matrix. Note that the Newton-Raphson method converges quickly and it requires reasonable initial values of states. In practice, the initial value of the state vector $\boldsymbol{x}^0$ can be set according to the system operating condition. Details on the selection of initial values can be found in section IV.

The parameters (including mutual inductances and capacitances) and the internal states ($\tilde{V}^1_{L_{tx1}}$, $\tilde{V}^1_{L_{tx2}}$, $\tilde{I}^1_{rx}$, $\tilde{U}^1$, $\tilde{V}^3_{L_{tx1}}$, $\tilde{V}^3_{L_{tx2}}$, $\tilde{I}^3_{rx}$ and $\tilde{U}^3$) are calculated simultaneously with (11). With the input voltages ($\tilde{U}^1$, $\tilde{U}^3$) and currents ($\tilde{I}^1_{rx}$, $\tilde{I}^3_{rx}$) of the rectifier, the equivalent input impedance of the rectifier R_{eq} can be calculated with $R_{eq} = U_1/I_{rx,1}$. U_1 and $I_{rx,1}$ are the magnitudes of $\tilde{U}^1$ and $\tilde{I}^1_{rx}$. The relationship between the equivalent impedance R_{eq} and the load R can be approximated based on the power equivalence principle as (12): the power dissipated on the resistance R is equal to the power provided by the fundamental and 3rd harmonic components of $u(t)$.

$$\left(U_1/\sqrt{2}\right)^2/R_{eq} + \left(U_3/\sqrt{2}\right)^2/R_{eq} = V_{out}^2/R \tag{12}$$

With the Fourier analysis of u(t) in (4) and the equivalent input impedance of the rectifier $R_{eq} = U_1/I_{rx,1}$, the load R can be directly calculated according to the fundamental frequency component at the input of the rectifier, i.e.,

$$R = (U_1/I_{rx,1})9\pi^2/80 \tag{13}$$

The flowchart of the proposed parameter identification method is shown in Fig. 3.

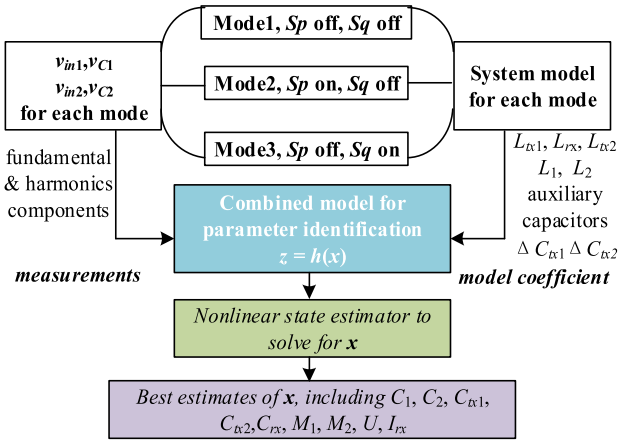

FIGURE 3. Flowchart of parameter identification method.

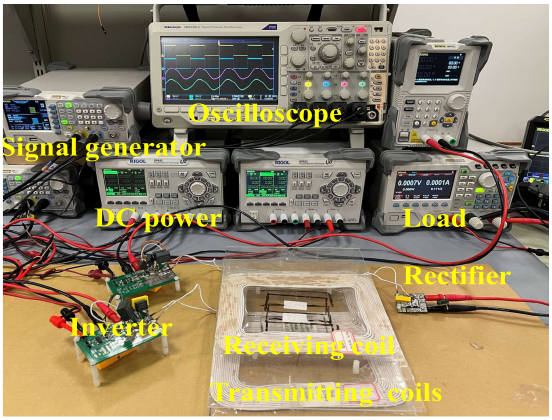

(a) Experimental platform

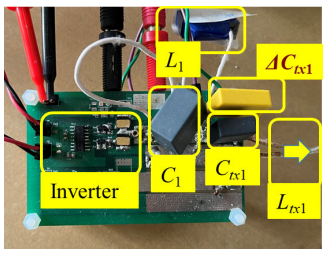

(b) Coupler design, transmitter #1

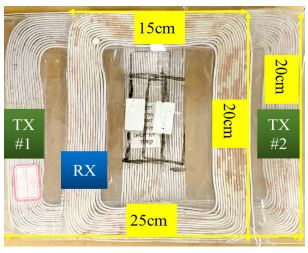

(c) Transmitting and receiving coil

FIGURE 4. Experimental setup of 2TX-1RX WPT system.

TABLE 2. System settings.

Transmitter #1 (TX1)	*Transmitter* #2 (TX2)	*Receiver* (RX)	*Nominal capacitor*
L_1= 29.63 μH	L_2= 25.96 μH		$\triangle C_{tx1}$ = 27 nF
C_1= 94 nF	C_2= 110 nF		$\triangle C_{tx2}$ = 22 nF
L_{tx1}= 58.28 μH	L_{tx2}= 59.86 μH	L_{rx}=60.47 μH	
C_{tx1}= 83 nF	C_{tx2}= 72 nF	C_{rx}= 42 nF	
r_{tx1}= 0.148 Ω	r_{tx2}=0.150 Ω	r_{rx}= 0.154 Ω	

IV. HARDWARE EXPERIMENTAL RESULTS

To verify the effectiveness of the proposed parameter identification method, a prototype 2TX-1RX LCC-S WPT system is established, as shown in Fig. 4 (a). The system topology is as same as that in Fig. 1. The designed ideal resonant frequency f_0 is 100 kHz and the experimental settings are shown in Table. 2.

The dc supplies are $V_{d1} = 30$ V and $V_{d2} = 30$ V. Here the operating frequency f is selected as 95 kHz, which is near but not exactly equal to the resonant frequency f_0 [21]. Through this selection of operating frequency, the independency among the parameters to be estimated can be guaranteed [21]. The duty cycle D of the switching signal for inverters is set as 0.494. Soft switching techniques (zero voltage switching) are adopted for both inverters in TX1 and TX2 to minimize the switching losses. The actual parameters of the components are measured offline by the LCR meter before the system starts. The transmitting coils and receiving coil are built using the Litz wire, with the same sizes (20 cm*15 cm) as shown in Fig.4 (c). The transmitting coils are positioned in bipolar pad form to decouple coils and minimize the cross coupling, i.e. $M_{12} = 0$ [38]. The receiving coil is centered on the top of the transmitting coils. Connect C_{tx1} and C_{tx2} in parallel with C_{tx1} and C_{tx2}, respectively. Fig.4 (b) shows the coupler design of transmitter #1 as an example. Here the auxiliary capacitors are chosen as MMK P82 and the values are $C_{tx1} = 27$ nF and $C_{tx2} = 22$ nF, which are close to 30% of capacitances C_{tx1} and C_{tx2}, respectively. The two auxiliary capacitors are with known and constant capacitances, and they only work for the purpose of parameter identification of the WPT system. Switch on/off the auxiliary capacitors C_{tx1} and C_{tx2} to generate three operating modes as introduced in section II of the paper.

Measurements for each mode contain the input voltages (v_{in1}, v_{in2}) and voltages across the capacitor (v_{C_1}, v_{C_2}). Since the experiments aim to verify the effectiveness and feasibility of the theoretical analysis for the proposed parameter identification method, here the oscilloscope (RIGOLMSO5104) is applied to collect the data for simplification [17], [25], [26].

The experiments include three cases to verify the effectiveness of the proposed parameter identification method. Case 1 verifies the effectiveness of the method with varying loads condition by ranging R from 15 Ω to 50 Ω. In case 2, the mutual inductances vary with different coils position, and

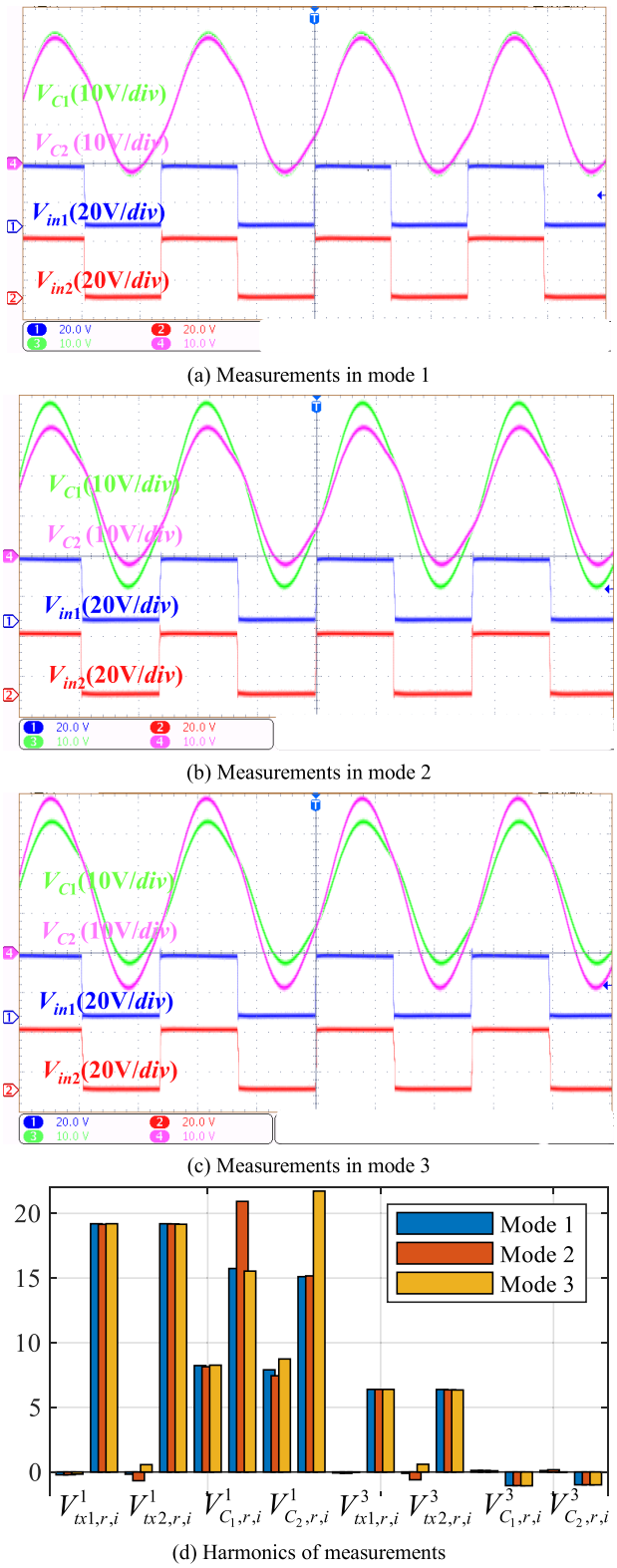

FIGURE 5. Measurements in mode (1) (2) (3), $R = 30$ Ω.

then the estimation method will be applied to identify the parameters of interest. Case 3 decreases the values of compensation capacitances to mimic the capacitor aging problem, and verifies the accuracy of the method in capacitor aging

conditions. Note that for the example WPT system, the rated dc output voltage and current are around 20 V and 1.5 A, respectively. The rated output power is 30 W. The WPT system can also be scaled up/down for various applications.

A. CASE 1 ESTIMATION WITH VARYING LOADS

In this case, the vertical distance between the transmitting coils and receiving coil is 2.2 cm. The actual mutual inductances are $M_1 = 16.736\ \mu$ H, $M_2 = 15.58\ \mu$ H and $M_{12} = 0$. The system configuration is the same as that in Table 2. Load R ranges from 15 Ω to 50 Ω, with the intervals of 5 Ω. An example case with $R = 30$ Ω, will be analyzed first. Fig. 5 shows the waveforms and the harmonic components of measurements for three modes when $R = 30$ Ω.

In Fig. 5, the waveforms and FFT analysis results of the measurements are different for different modes. In Fig. 5 (a) to (c), the input voltage (V_{in1} or V_{in2}) and the capacitor voltage (V_{C_1} or V_{C_2}) are shown for each transmitter (TX1 or TX2). One can observe that the capacitor voltages are not pure sinusoids since they contain harmonics. Also, one can observe that, V_{C_1} increases by comparing mode 1 and mode 2, and V_{C_2} increases by comparing mode 1 and mode 3. This is because the introduction of capacitors causes deviation of the resonant frequency from its nominal value. This also shows that the introduction of auxiliary capacitors provides more information for the parameter identification problem.

Next, the way to select the initial value of the state vector for the Newton Raphson method in (11) is presented. There are 55 states of the system, including 7 parameters and 48 (16*3) internal states corresponding to three modes. The initial value of each state is set within certain boundaries considering the operating condition of the system. Considering the ranges of the coupling coefficient from 0.1 to 0.5, the initial values of mutual inductances M_1 and M_2 are selected within the range from 6 μH to 30 μH. The initial values of capacitors C_1, C_2, C_{tx1}, C_{tx2}, C_{rx} are set close to their nominal values, without knowing the degradation status of the capacitors. The 48 (16*3) internal states of three modes can be set within certain ranges: $U_1 \in$ [10 V, 40 V], $U_3 \in$ [3 V, 13 V], $\theta_1, \theta_3 \in [-\pi/2, \pi/2]$, $I^1_{rx,r}, I^1_{rx,i} \in$ [−2 A, 2 A] and $I^{3rd}_{rx,r}, I^{3rd}_{rx,i} \in$ [−0.2 A, 0.2 A]. The values of $V^1_{L_{tx1},r}$, $V^1_{L_{tx1},i}$, $V^{3rd}_{L_{tx1},r}$, $V^{3rd}_{L_{tx1},i}$, $V^1_{L_{tx2},r}$, $V^1_{L_{tx2},i}$, $V^{3rd}_{L_{tx2},r}$, and $V^{3rd}_{L_{tx2},i}$ of each mode can be approximated using the fundamental and 3rd harmonics components of measurements V_{C_1} and V_{C_2}. In this paper, the Newton Raphson method in (11) has a relatively large convergence region for the WPT parameter identification application. Experimental results prove that, with the aforementioned ways of selecting the initial values, as long as the initial values are selected with the boundary, the proposed method does not encounter convergence issues.

Substitute the harmonic components and the initial state vector $\boldsymbol{x}^0$ into the parameter identification model (9), the states can be solved. The convergence procedure of the parameters is shown in Fig. 6 and Fig.7. It can be seen that the value of the optimal parameters will be determined after a few steps. The estimated parameters are, $M_1 = 16.68\ \mu$H, $M_2 = 15.72\ \mu$H, $C_1 = 94.97$ nF, $C_2 = 109.6$ nF, $C_{tx1} = 85.13$ nF, $C_{tx2} = 72.39$ nF, and $C_{rx} = 41.3$ nF. With the estimated load voltages and currents, the value of load R can be calculated according to (13), i.e. $R = 30.88$ Ω. Compared to the actual values, the absolute estimation error is calculated

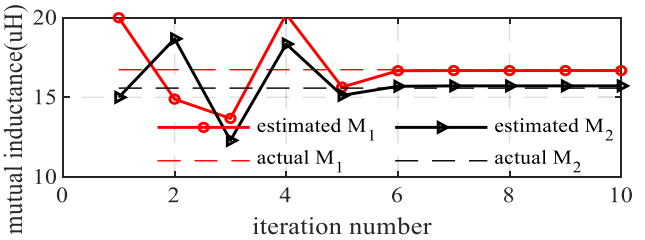

FIGURE 6. Convergence of mutual inductances, $R = 30$ Ω.

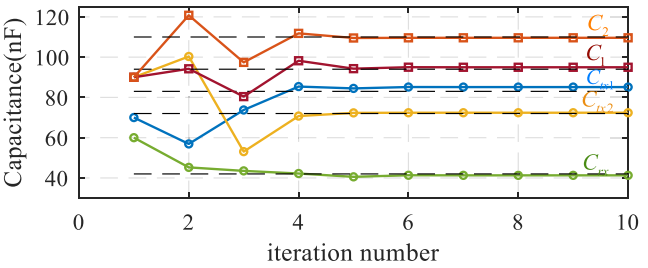

FIGURE 7. Convergence of capacitances, $R = 30$ Ω.

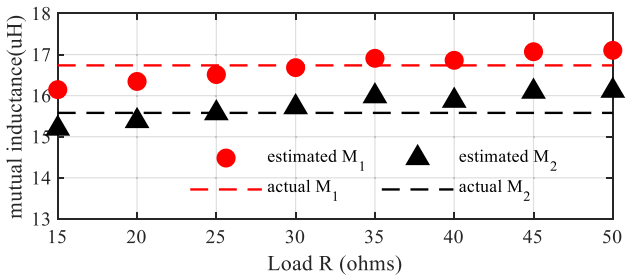

FIGURE 8. Estimation results of mutual inductances, varying R.

TABLE 3. Estimation error for capacitances, $R = 30$ Ω.

Capacitance	C_1	C_{tx1}	C_2	C_{tx2}	C_{rx}
Error (%)	1.03	2.56	0.36	0.54	1.68

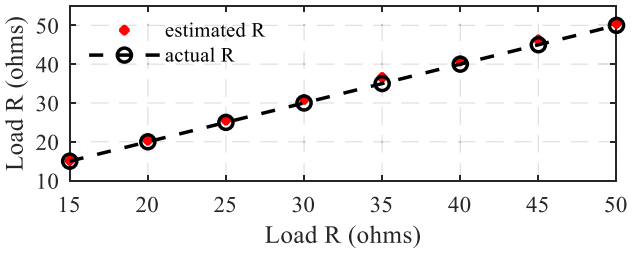

FIGURE 9. Estimation results of load R, varying R.

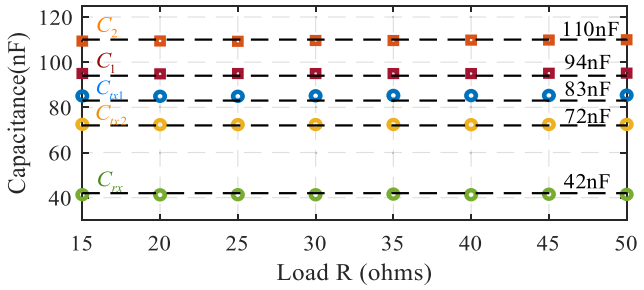

FIGURE 10. Estimation results of capacitances, varying *R*.

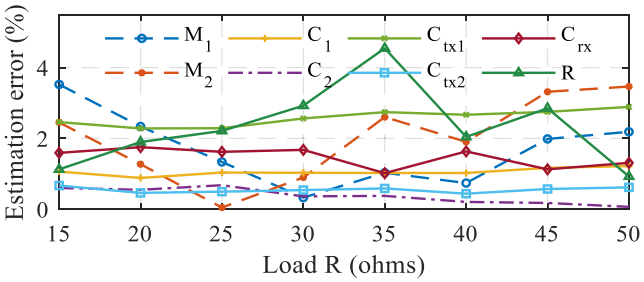

FIGURE 11. Estimation error of parameters, varying *R*.

TABLE 4. Estimation error, varying load *R*.

Error	M_1	M_2	C_1	C_{tx1}	C_2	C_{tx2}	C_{rx}	R
Avg (%)	1.68	1.99	1.05	2.58	0.38	0.55	1.47	2.32
Max (%)	3.52	3.47	1.22	2.89	0.68	0.67	1.75	4.55

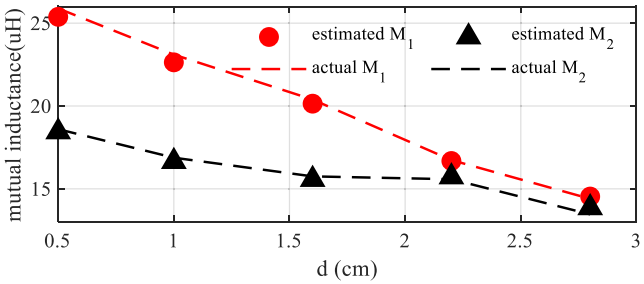

FIGURE 12. Estimation results of mutual inductances, varying *M*.

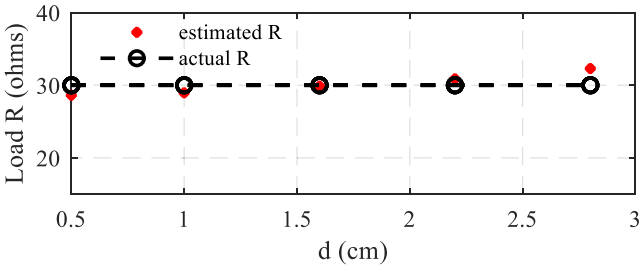

FIGURE 13. Estimation results of load *R*, varying *M*.

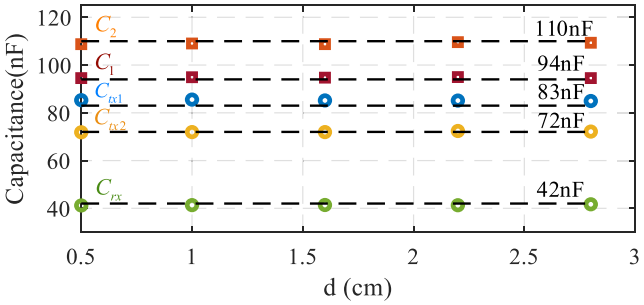

FIGURE 14. Estimation results of capacitances, varying *M*.

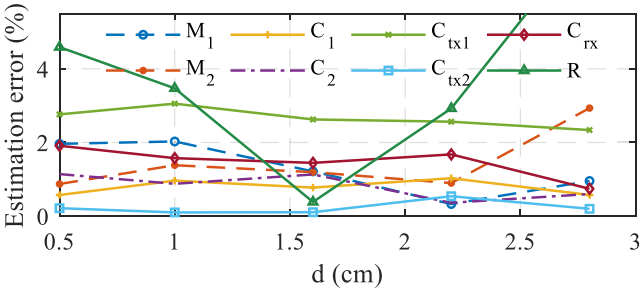

FIGURE 15. Estimation error of states, varying M.

TABLE 5. Estimation error, varying mutual inductances.

Error	M_1	M_2	C_1	C_{tx1}	C_2	C_{tx2}	C_{rx}	R
Avg (%)	1.3	1.46	0.78	2.67	0.82	0.23	1.47	3.8
Max (%)	2.03	2.93	1.03	3.05	1.14	0.54	1.91	7.66

as $Error = |estimated - actual|/actual \times 100\%$. The estimation errors for M_1 and M_2 are 0.3% and 0.9%, respectively. The estimation error for load R is 2.93 %. The estimation errors for the capacitances are shown in Table 3. One can observe that the estimated parameters are with high accuracy.

To further verify the effectiveness of the proposed method, here set the load R varying from 15 to 50 Ω with the interval 5 Ω. When the load varies, the system operating condition will change. Fig. 8 shows the estimation results of mutual inductances with unknown varying R. In Fig. 8, red circles and black triangles represent estimated M_1 and M_2, respectively. Fig. 9 and Fig. 10 show the estimation results of load R and capacitances (C_1, C_2, C_{tx1}, C_{tx2}, and C_{rx}). The estimated values are also close to the actual values with different loads. The estimation results show that the method can work for various loading conditions since $\tilde{U}^{n^{th}}$ and $\tilde{I}_{rx}^{n^{th}}$ have been included in the model and the variation of R is carefully considered.

Fig. 11 shows the estimation error (in percentage) of all the parameters of interest. The maximum and average estimation errors of the case with varying R are shown in Table 4. It can be seen that the maximum parameter identification error is around 3.5% for mutual inductances, 2.9% for capacitances, and 4.55% for loads. The results verified that the mutual inductances, the load, and the capacitances can be accurately estimated simultaneously. Note that, the estimation errors of

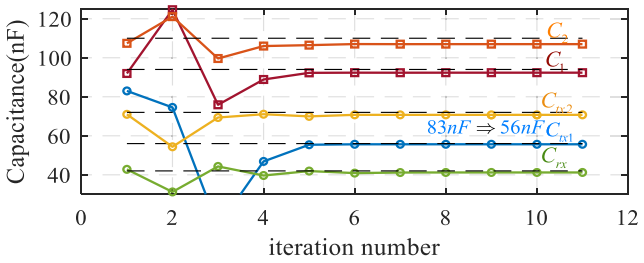

FIGURE 16. Estimation of capacitances, C_{tx1} degrading from 83 nF to 56 nF.

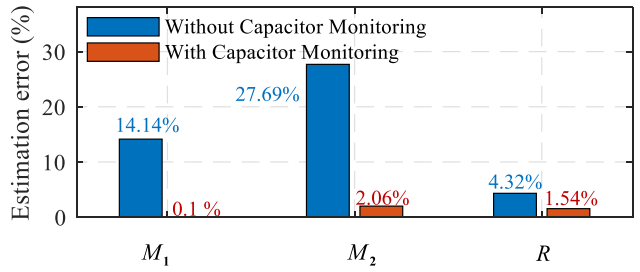

FIGURE 17. Comparison of estimation errors with/without capacitor monitoring.

loads are a bit larger than other parameters. The reason is that the forward voltage drop of diodes in the rectifier has not been considered when calculating the load with states $\tilde{U}^1$ and $\tilde{I}^1_{rx}$ in (13).

B. CASE 2 ESTIMATION WITH VARYING MUTUAL INDUCTANCES

In this case, the load is fixed as 30 Ω. The vertical distance between the transmitting coils and receiving coil ranges from 0.5 cm to 2.8 cm. The mutual inductances M_1 and M_2 change with different distances. The other settings are the same as those in Table 2. For each pair of mutual inductances with a certain vertical distance, switch the auxiliary capacitors and include the measurements of three modes within the model. Finally, the estimation results are shown in Fig. 12 to Fig. 14.

In Fig. 12, red circles and black triangles represent estimated M_1 and M_2, respectively. When the distance changes, the actual mutual inductances change. Similarly, the estimated values are always close to the actual mutual inductances. Fig. 13 and 14 show the estimation results of load R and capacitances C_1, C_2, C_{tx1}, C_{tx2}, and C_{rx}. The estimated values are consistent with the actual values with varying mutual inductances.

The estimation errors for parameters (M_1, M_2, C_1, C_2, C_{tx1}, C_{tx2}, C_{rx}, and R) are shown in Fig. 15. The average and maximum absolute estimation errors for parameters are shown in Table 5.

The maximum absolute estimation error is around 3% for mutual inductances and 3% for capacitances. It can be seen, all the estimation errors for load R are smaller than 5% except in the case when distance $d = 2.8$ cm (with the error of 7.66%), meaning the calculation procedure for R could be further compromised with weak coupling. The estimation error of R is also contributed by the neglection of voltage drop of diodes during derivation. Overall, the estimation results still show that the proposed method can work when the coil distance varies.

C. CASE 3 ESTIMATION WITH AGING CAPACITOR

In this case, the capacitance C_{tx1} ranges from 83 nF to 56 nF to mimic the capacitor aging. The load R equals to 30 Ω. The distance between the transmitting coils and receiving coil is fixed at 1.6 cm as an example. The actual mutual inductances are $M_1 = 20.39$ μH and $M_2 = 15.75$ μH. With the proposed method, the estimation results for mutual inductances and load R are $M_1 = 20.41$ μH (0.1% error), $M_2 = 15.43$ μH (2.06% error), $R = 28.70$ Ω (1.54% error). The capacitor monitoring results with the proposed method are shown in Fig. 16. One can observe that, even with the initial value around 83 nF, C_{tx1} still converges to the value of 55.6 nF, which is close to the true value of 56 nF (0.7% error). The degradation of C_{tx1} is accurately detected with the proposed method.

Next, a comparative study is provided, where the estimation method does not consider the capacitance uncertainties. The proposed method is adjusted such that all the values of capacitances are removed from the unknown state vector and are treated as known constants with values in Table 2. That is to say, the value of C_{tx1} is fixed as 83 nF in the model even though it has already been degraded to 56 nF. Under this condition, the estimation results of mutual inductances and load are $M_1 = 22.98$ μH (14.14% error), $M_2 = 11.25$ μH (27.69% error) and $R = 32.53$ Ω (4.32% error), with much larger errors than the proposed method. The estimation errors of mutual inductances and load with and without consideration of capacitance uncertainties are shown in Fig. 17.

When the system operates with the degraded capacitor, the estimation accuracy of parameters and operating conditions for the WPT system could be compromised. From the result, it can be seen that, when the capacitor aging is modeled in the parameter identification method, the estimation accuracy is much improved.

V. DISCUSSION

This section shows additional discussions for the proposed method, including a comparison to other estimation methods and other discussions.

A. COMPARISON TO OTHER ESTIMATION METHODS

The existing estimation methods for identifying parameters in WPT systems usually require frequency sweeping, energy injection, and communication from the receiver side. Also, most methods are only designed for 1TX/RX WPT systems or do not consider the uncertainty of capacitor parameters. The advantages of the proposed method over existing methods are summarized in Table 6.

B. OTHER DISCUSSIONS

In this paper, the parameters can be accurately estimated with various mutual inductances and loads, with uncertain

TABLE 6. Comparison to other parameter identification methods.

Features / Ref	No frequency sweeping	No energy injection	No communication from receiver	Identify both M & load	Monitor capacitors	Multi-TX/RX
[14-15]	√	×	√	×	×	×
[16-18]	√	√	√	×	×	×
[19-22]	√	√	√	√	×	×
[24-25]	√	√	√	√	√	×
[26]	×	√	√	√	√	√
[27-30]	√	√	×	√	×	√
Proposed	√	√	√	√	√	√

capacitances. It is worth mentioning that those parameters may not be accurately captured in extreme scenarios. For example, when the load resistance goes to infinity, the receiving side of the WPT system becomes an open circuit. In this case, it is obvious that the mutual inductances cannot be accurately captured, since the input current will be zero regardless of the mutual inductances.

Accurate estimation of parameters can potentially enable many applications, such as constant output voltage/current control or maximum transfer efficiency control. Taking the maximum transfer efficiency control as an example. With the estimated mutual inductances M_1 and M_2, the optimal efficiency can be obtained by setting the coil current ratio as the coupling coefficient ratio, as $I_{tx1}{:}I_{tx2} = k_1{:}k_2 = (M_1/\sqrt{L_{tx1}L_{rx}}){:}(M_2/\sqrt{L_{tx2}L_{rx}})$ [28]. Since the focus of the paper is parameter identification, details experimental results of those applications are not demonstrated due to space limitations.

This study introduces a parameter identification method for 2TX-1RX LCC-S compensated WPT systems. The proposed method provides a theoretical framework for estimating the parameters systematically. As a result, the method can be potentially extended to other multi-coil WPT systems, with different compensation topologies and different number of TXs/RXs. However, if the system contains more TXs/RXs, the number of measurements and the unknown variables could also be increased, resulting in a more complex formulation of the parameter identification problem. Also, for each application scenario, the information redundancy and parameter independence should be checked carefully to ensure all the parameters of interest can be identified simultaneously.

Although the proposed approach is validated via a WPT system with the resonant frequency of 100 kHz as an example, similar approaches can also be applied to WPT systems with higher resonant frequencies. However, in those cases, the parasitic parameters of the circuit elements could be more influential and are suggested to be considered. In addition, advanced voltage sensors that are compatible with higher sampling rates and wider bandwidth should be considered.

VI. CONCLUSION

This paper proposed a parameter identification method for 2TX-1RX LCC-S WPT systems, to estimate the mutual inductances, load, and capacitances at the same time. The method only requires voltage measurements at the transmitter side and does not need information from the receiver side. To improve the redundancy of the parameter identification problem, the proposed method utilizes auxiliary capacitors to make the system work at different operating modes. First, the model for each operating mode is established with fundamental and high-order harmonic information. Afterward, an overall model combining the information from all three operating modes is derived. Finally, a nonlinear state estimator is applied to solve the nonlinear model numerically. Hardware experiments verified that the proposed method can accurately estimate mutual inductances, load, and capacitances simultaneously, during different operating conditions with various loads, mutual inductances, and capacitor aging scenarios. Accurate identification of those parameters enables highly efficient, controllable and reliable operation for WPT systems.

REFERENCES

[1] Z. Zhang, H. Pang, A. Georgiadis, and C. Cecati, "Wireless power transfer—An overview," *IEEE Trans. Ind. Electron.*, vol. 66, no. 2, pp. 1044–1058, Feb. 2019.

[2] D. Patil, M. K. McDonough, J. M. Miller, B. Fahimi, and P. T. Balsara, "Wireless power transfer for vehicular applications: Overview and challenges," *IEEE Trans. Transport. Electrific.*, vol. 4, no. 1, pp. 3–37, Mar. 2018.

[3] S. C. Tang, T. L. T. Lun, Z. Guo, K.-W. Kwok, and N. J. McDannold, "Intermediate range wireless power transfer with segmented coil transmitters for implantable heart pumps," *IEEE Trans. Power Electron.*, vol. 32, no. 5, pp. 3844–3857, May 2017.

[4] G. A. Covic, J. T. Boys, M. L. G. Kissin, and H. G. Lu, "A three-phase inductive power transfer system for roadway-powered vehicles," *IEEE Trans. Ind. Electron.*, vol. 54, no. 6, pp. 3370–3378, Dec. 2007.

[5] V.-B. Vu, D.-H. Tran, and W. Choi, "Implementation of the constant current and constant voltage charge of inductive power transfer systems with the double-sided LCC compensation topology for electric vehicle battery charge applications," *IEEE Trans. Power Electron.*, vol. 33, no. 9, pp. 7398–7410, Sep. 2018.

[6] M. Fu, H. Yin, M. Liu, and C. Ma, "Loading and power control for a high-efficiency class E PA-driven megahertz WPT system," *IEEE Trans. Ind. Electron.*, vol. 63, no. 11, pp. 6867–6876, Nov. 2016.

[7] Y. Guo, Y. Zhang, W. Zhang, and L. Wang, "Battery parameter identification based on wireless power transfer system with rectifier load," *IEEE Trans. Ind. Electron.*, vol. 68, no. 8, pp. 6893–6904, Aug. 2021.

[8] W. Zhong and S. Y. R. Hui, "Maximum energy efficiency operation of series-series resonant wireless power transfer systems using on-off keying modulation," *IEEE Trans. Power Electron.*, vol. 33, no. 4, pp. 3595–3603, Apr. 2018.

[9] Z. Huang, S.-C. Wong, and C. K. Tse, "Control design for optimizing efficiency in inductive power transfer systems," *IEEE Trans. Power Electron.*, vol. 33, no. 5, pp. 4523–4534, May 2018.

[10] X. Dai, X. Li, Y. Li, and A. P. Hu, "Maximum efficiency tracking for wireless power transfer systems with dynamic coupling coefficient estimation," *IEEE Trans. Power Electron.*, vol. 33, no. 6, pp. 5005–5015, Jun. 2018.

[11] C. Lv, J. Liu, Y. Zhang, J. Yin, R. Cao, Y. Li, and X. Liu, "A method to characterize the shrinking of safe operation area of metallized film capacitor considering electrothermal coupling and aging in power electronics applications," *IEEE Trans. Ind. Electron.*, vol. 70, no. 2, pp. 1993–2002, Feb. 2023.

[12] J. Xu, L. Gu, and J. Rivas-Davila, "Effect of class 2 ceramic capacitor variations on switched-capacitor and resonant switched-capacitor converters," *IEEE J. Emerg. Sel. Topics Power Electron.*, vol. 8, no. 3, pp. 2268–2275, Sep. 2020.

[13] Y. Wang, Z. Yang, and F. Lin, "Design and implementation of wireless power transfer systems with improved capacitor error tolerance," *IEEE Trans. Ind. Electron.*, vol. 69, no. 5, pp. 4707–4717, May 2022.

[14] S. Hu, Z. Liang, Y. Wang, J. Zhou, and X. He, "Principle and application of the contactless load detection based on the amplitude decay rate in a transient process," *IEEE Trans. Power Electron.*, vol. 32, no. 11, pp. 8936–8944, Nov. 2017.
[15] Z. H. Wang, Y. P. Li, Y. Sun, C. S. Tang, and X. Lv, "Load detection model of voltage-fed inductive power transfer system," *IEEE Trans. Power Electron.*, vol. 28, no. 11, pp. 5233–5243, Nov. 2013.
[16] M. Mohammad and S. Choi, "Sensorless estimation of coupling coefficient based on current and voltage harmonics analysis for wireless charging system," in *Proc. IEEE Energy Convers. Congr. Exposit. (ECCE)*, Cincinnati, OH, USA, Oct. 2017, pp. 2767–2772.
[17] J. P.-W. Chow, H. S.-H. Chung, and C.-S. Cheng, "Use of transmitter-side electrical information to estimate mutual inductance and regulate receiver-side power in wireless inductive link," *IEEE Trans. Power Electron.*, vol. 31, no. 9, pp. 6079–6091, Sep. 2016.
[18] K. Yue, Y. Liu, P. Zhao, B. Xue, and R. He, "Time domain coupling coefficient estimation using transmitter-side information in wireless power transfer system," in *Proc. 45th Annu. Conf. IEEE Ind. Electron. Soc.*, Oct. 2019, pp. 4189–4194.
[19] X. Sheng and L. Shi, "Mutual inductance and load identification method for inductively coupled power transfer system based on auxiliary inverter," *IEEE Trans. Veh. Technol.*, vol. 69, no. 2, pp. 1533–1541, Feb. 2020.
[20] Y. G. Su, H. Y. Zhang, Z. H. Wang, A. P. Hu, L. Chen, and Y. Sun, "Steady-state load identification method of inductive power transfer system based on switching capacitors," *IEEE Trans. Power Electron.*, vol. 30, no. 11, pp. 6349–6355, Nov. 2015.
[21] J. Yin, D. Lin, T. Parisini, and S. Y. R. Hui, "Front-end monitoring of the mutual inductance and load resistance in a series-series compensated wireless power transfer system," *IEEE Trans. Power Electron.*, vol. 31, no. 10, pp. 7339–7352, Oct. 2016.
[22] Y. Yang, Y. Jiang, S.-C. Tan, and S.-Y.-R. Hui, "A frequency-sweep based load monitoring method for weakly-coupled series-series compensated wireless power transfer systems," in *Proc. IEEE PELS Workshop Emerg. Technologies, Wireless Power Transf. (Wow)*, Montréal, QC, Jun. 2018, pp. 1–5.
[23] J. Hu, J. Zhao, and C. Cui, "A wide charging range wireless power transfer control system with harmonic current to estimate the coupling coefficient," *IEEE Trans. Power Electron.*, vol. 36, no. 5, pp. 5082–5094, May 2021.
[24] J. Liu, G. Wang, G. Xu, J. Peng, and H. Jiang, "A parameter identification approach with primary-side measurement for DC–DC wireless-power-transfer converters with different resonant tank topologies," *IEEE Trans. Transport. Electrific.*, vol. 7, no. 3, pp. 1219–1235, Sep. 2021.
[25] R. Dai, W. Zhou, Y. Chen, Z. Zhu, and R. Mai, "Pulse density modulation based mutual inductance and load resistance identification method for wireless power transfer system," *IEEE Trans. Power Electron.*, vol. 37, no. 8, pp. 9933–9943, Aug. 2022.
[26] Y. Yang, S.-C. Tan, and S. Y. R. Hui, "Front-end parameter monitoring method based on two-layer adaptive differential evolution for SS-compensated wireless power transfer systems," *IEEE Trans. Ind. Informat.*, vol. 15, no. 11, pp. 6101–6113, Nov. 2019.
[27] D.-H. Kim and D. Ahn, "Maximum efficiency point tracking for multiple-transmitter wireless power transfer," *IEEE Trans. Power Electron.*, vol. 35, no. 11, pp. 11391–11400, Nov. 2020.
[28] S. Huh and D. Ahn, "Two-transmitter wireless power transfer with optimal activation and current selection of transmitters," *IEEE Trans. Power Electron.*, vol. 33, no. 6, pp. 4957–4967, Jun. 2018.
[29] D.-H. Kim, S. Kim, S.-W. Kim, J. Moon, I. Cho, and D. Ahn, "Coupling extraction and maximum efficiency tracking for multiple concurrent transmitters in dynamic wireless charging," *IEEE Trans. Power Electron.*, vol. 35, no. 8, pp. 7853–7862, Aug. 2020.
[30] X. Dai, J.-C. Jiang, and J.-Q. Wu, "Charging area determining and power enhancement method for multiexcitation unit configuration of wirelessly dynamic charging EV system," *IEEE Trans. Ind. Electron.*, vol. 66, no. 5, pp. 4086–4096, May 2019.
[31] S. Yang, D. Xiang, A. Bryant, P. Mawby, L. Ran, and P. Tavner, "Condition monitoring for device reliability in power electronic converters: A review," *IEEE Trans. Power Electron.*, vol. 25, no. 11, pp. 2734–2752, Nov. 2010.
[32] J. Poon, P. Jain, I. C. Konstantakopoulos, C. Spanos, S. K. Panda, and S. R. Sander, "Model-based fault detection and identification for switching power converters," *IEEE Trans. Power Electron.*, vol. 32, no. 2, pp. 1419–1430, Feb. 2017.
[33] K. Yue, Y. Liu, P. Zhao, B. Wang, M. Fu, and H. Wang, "Dynamic state estimation enabled health indicator for parametric fault detection in switching power converters," *IEEE Access*, vol. 9, pp. 33224–33234, 2021.
[34] J. Poon, P. Jain, C. Spanos, S. K. Panda, and S. R. Sanders, "Fault prognosis for power electronics systems using adaptive parameter identification," *IEEE Trans. Ind. Appl.*, vol. 53, no. 3, pp. 2862–2870, May 2017.
[35] M. Ahmeid, M. Armstrong, S. Gadoue, M. Al-Greer, and P. Missailidis, "Real-time parameter estimation of DC–DC converters using a self-tuned Kalman filter," *IEEE Trans. Power Electron.*, vol. 32, no. 7, pp. 5666–5674, Jul. 2017.
[36] M. A. Vogelsberger, T. Wiesinger, and H. Ertl, "Life-cycle monitoring and voltage-managing unit for DC-link electrolytic capacitors in PWM converters," *IEEE Trans. Power Electron.*, vol. 26, no. 2, pp. 493–503, Feb. 2011.
[37] W. Xiao, R. Shen, B. Zhang, D. Qiu, Y. Chen, and F. Xie, "Multiple parameters estimation based on transmitter side information in wireless power transfer system," *IEEE Access*, vol. 7, pp. 164835–164843, 2019.
[38] A. Zaheer, G. A. Covic, and D. Kacprzak, "A bipolar pad in a 10-kHz 300-W distributed IPT system for AGV applications," *IEEE Trans. Ind. Electron.*, vol. 61, no. 7, pp. 3288–3301, Jul. 2014.
[39] V. J. Chin, Z. Salam, and K. Ishaque, "An accurate and fast computational algorithm for the two-diode model of PV module based on a hybrid method," *IEEE Trans. Ind. Electron.*, vol. 64, no. 8, pp. 6212–6222, Aug. 2017.
[40] Y. Chen and V. Dinavahi, "An iterative real-time nonlinear electromagnetic transient solver on FPGA," *IEEE Trans. Ind. Electron.*, vol. 58, no. 6, pp. 2547–2555, Jun. 2011.

KANG YUE (Student Member, IEEE) received the B.S. degree in electrical engineering and its automation from the Hefei University of Technology, Hefei, China, in 2017. She is currently pursuing the Ph.D. degree with the Power System Protection and Automation Laboratory, School of Information Science and Technology, ShanghaiTech University. Her research interests include health monitoring and parameter identification of power electronic systems.

YU LIU (Senior Member, IEEE) received the B.S. and M.S. degrees in electrical power engineering from Shanghai Jiao Tong University, Shanghai, China, in 2011 and 2013, respectively, and the Ph.D. degree in electrical and computer engineering from the Georgia Institute of Technology, Atlanta, GA, USA, in 2017. He is currently a tenure-track Assistant Professor with the School of Information Science and Technology, ShanghaiTech University, Shanghai. He has authored or coauthored three book chapters and more than 90 technical articles. His research interests include modeling, protection, fault location, and the state/parameter estimation of power systems and power electronic systems. He was a recipient of the 2022 IEEE PES Technical Committee Working Group Recognition Award for Outstanding Technical Report. He was also a recipient of the Shanghai Eastern Scholar Professorship and the Shanghai Pujiang Scholar. He serves as an Associate Editor for *IET Renewable Power Generation* (RPG) and a Guest Editor for the *Journal of Modern Power Systems and Clean Energy* (MPCE).

MINFAN FU (Senior Member, IEEE) received the B.S., M.S., and Ph.D. degrees in electrical and computer engineering from the University of Michigan–Shanghai Jiao Tong University Joint Institute, Shanghai Jiao Tong University, Shanghai, China, in 2010, 2013, and 2016, respectively.

From 2016 to 2018, he was a Postdoctoral Researcher with the Center for Power Electronics Systems (CPES), Virginia Polytechnic Institute and State University, Blacksburg, VA, USA. He is currently an Assistant Professor with the School of Information Science and Technology, ShanghaiTech University, Shanghai. He holds one U.S. patent, 15 Chinese patents, and has authored or coauthored more than 100 papers in prestigious IEEE journals and conferences. His research interests include wireless power transfer, high-frequency power conversion, high-frequency magnetic design, and the application of wide-bandgap devices.

Dr. Fu serves as the Organization Chair for ICWPT, ICIT, and ASSIST. He is also an Associate Editor of *IEEE IES Industrial Electronics Technology News* (ITeN).

JUNRUI LIANG (Senior Member, IEEE) received the B.E. and M.E. degrees in instrumentation engineering from Shanghai Jiao Tong University, Shanghai, China, in 2004 and 2007, respectively, and the Ph.D. degree in mechanical and automation engineering from The Chinese University Hong Kong, Hong Kong, SAR, China, in 2010.

He is currently an Associate Professor with the School of Information Science and Technology, ShanghaiTech University, Shanghai. His research interests include energy conversion and power conditioning circuits, kinetic energy harvesting and vibration suppression, the IoT devices, and mechatronics. He was a recipient of three best paper awards at the 2009 and 2010 IEEE International Conference on Information and Automation and the 2021 International Conference on Vibration Energy Harvesting and Applications. He is the General Chair of the Second International Conference on Vibration and Energy Harvesting Applications (VEH), in 2019. He is an Associate Editor of *IET Circuits, Devices and Systems*.

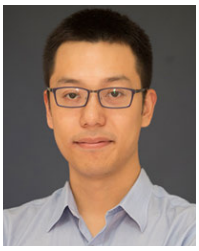

HAOYU WANG (Senior Member, IEEE) received the bachelor's degree (Hons.) in electrical engineering from Zhejiang University, Hangzhou, China, in 2009, and the Ph.D. degree in electrical engineering from the University of Maryland at College Park, College Park, MD, USA, in 2014.

In September 2014, he joined the School of Information Science and Technology, ShanghaiTech University, Shanghai, China, where he is currently a tenured Associate Professor. His research interests include power electronics, plug-in electric and hybrid electric vehicles, the applications of wide-bandgap semiconductors, renewable energy harvesting, and power management integrated circuits. He is an Associate Editor of IEEE TRANSACTIONS ON INDUSTRIAL ELECTRONICS, IEEE TRANSACTIONS ON TRANSPORTATION ELECTRIFICATION, and *CPSS Transactions on Power Electronics and Applications*.